



Weight Assessment for Fuselage Shielding on Aircraft With Open-Rotor Engines and Composite Blade Loss

*Kelly Carney, Michael Pereira, Lee Kohlman, Robert Goldberg, Edmane Envia,
Charles Lawrence, and Gary Roberts
Glenn Research Center, Cleveland, Ohio*

*William Emmerling
FAA William J. Hughes Technical Center, Atlantic City, New Jersey*

NASA STI Program . . . in Profile

Since its founding, NASA has been dedicated to the advancement of aeronautics and space science. The NASA Scientific and Technical Information (STI) program plays a key part in helping NASA maintain this important role.

The NASA STI Program operates under the auspices of the Agency Chief Information Officer. It collects, organizes, provides for archiving, and disseminates NASA's STI. The NASA STI program provides access to the NASA Aeronautics and Space Database and its public interface, the NASA Technical Reports Server, thus providing one of the largest collections of aeronautical and space science STI in the world. Results are published in both non-NASA channels and by NASA in the NASA STI Report Series, which includes the following report types:

- **TECHNICAL PUBLICATION.** Reports of completed research or a major significant phase of research that present the results of NASA programs and include extensive data or theoretical analysis. Includes compilations of significant scientific and technical data and information deemed to be of continuing reference value. NASA counterpart of peer-reviewed formal professional papers but has less stringent limitations on manuscript length and extent of graphic presentations.
- **TECHNICAL MEMORANDUM.** Scientific and technical findings that are preliminary or of specialized interest, e.g., quick release reports, working papers, and bibliographies that contain minimal annotation. Does not contain extensive analysis.
- **CONTRACTOR REPORT.** Scientific and technical findings by NASA-sponsored contractors and grantees.

- **CONFERENCE PUBLICATION.** Collected papers from scientific and technical conferences, symposia, seminars, or other meetings sponsored or cosponsored by NASA.
- **SPECIAL PUBLICATION.** Scientific, technical, or historical information from NASA programs, projects, and missions, often concerned with subjects having substantial public interest.
- **TECHNICAL TRANSLATION.** English-language translations of foreign scientific and technical material pertinent to NASA's mission.

Specialized services also include creating custom thesauri, building customized databases, organizing and publishing research results.

For more information about the NASA STI program, see the following:

- Access the NASA STI program home page at <http://www.sti.nasa.gov>
- E-mail your question to help@sti.nasa.gov
- Fax your question to the NASA STI Information Desk at 443-757-5803
- Phone the NASA STI Information Desk at 443-757-5802
- Write to:
STI Information Desk
NASA Center for AeroSpace Information
7115 Standard Drive
Hanover, MD 21076-1320



Weight Assessment for Fuselage Shielding on Aircraft With Open-Rotor Engines and Composite Blade Loss

*Kelly Carney, Michael Pereira, Lee Kohlman, Robert Goldberg, Edmane Envia,
Charles Lawrence, and Gary Roberts
Glenn Research Center, Cleveland, Ohio*

*William Emmerling
FAA William J. Hughes Technical Center, Atlantic City, New Jersey*

National Aeronautics and
Space Administration

Glenn Research Center
Cleveland, Ohio 44135

Trade names and trademarks are used in this report for identification only. Their usage does not constitute an official endorsement, either expressed or implied, by the National Aeronautics and Space Administration.

Level of Review: This material has been technically reviewed by technical management.

Available from

NASA Center for Aerospace Information
7115 Standard Drive
Hanover, MD 21076-1320

National Technical Information Service
5301 Shawnee Road
Alexandria, VA 22312

Available electronically at <http://www.sti.nasa.gov>

Weight Assessment for Fuselage Shielding on Aircraft With Open-Rotor Engines and Composite Blade Loss

Kelly Carney, Michael Pereira, Lee Kohlman, Robert Goldberg, Edmane Envia,
Charles Lawrence, and Gary Roberts
National Aeronautics and Space Administration
Glenn Research Center
Cleveland, Ohio 44135

William Emmerling
FAA William J. Hughes Technical Center
Atlantic City, New Jersey 08234

Abstract

The Federal Aviation Administration (FAA) has been engaged in discussions with airframe and engine manufacturers concerning regulations that would apply to new technology fuel efficient “open-rotor” engines. Existing regulations for the engines and airframe did not envision features of these engines that include eliminating the fan blade containment systems and including two rows of counter-rotating blades. Damage to the airframe from a failed blade could potentially be catastrophic. Therefore the feasibility of using aircraft fuselage shielding was investigated. In order to establish the feasibility of this shielding, a study was conducted to provide an estimate for the fuselage shielding weight required to provide protection from an open-rotor blade loss. This estimate was generated using a two-step procedure. First, a trajectory analysis was performed to determine the blade orientation and velocity at the point of impact with the fuselage. The trajectory analysis also showed that a blade dispersion angle of $\pm 3^\circ$ bounded the probable dispersion pattern and so was used for the weight estimate. Next, a finite element impact analysis was performed to determine the required shielding thickness to prevent fuselage penetration. The impact analysis was conducted using an FAA-provided composite blade geometry. The fuselage geometry was based on a medium-sized passenger composite airframe. In the analysis, both the blade and fuselage were assumed to be constructed from a T700S/PR520 triaxially-braided composite architecture. Sufficient test data on T700S/PR520 is available to enable reliable analysis, and also demonstrate its good impact resistance properties. This system was also used in modeling the surrogate blade. The estimated additional weight required for fuselage shielding for a wing-mounted counter-rotating open-rotor blade is 236 lb per aircraft. This estimate is based on the shielding material serving the dual use of shielding and fuselage structure. If the shielding material is not used for dual purpose, and is only used for shielding, then the additional weight per aircraft is estimated to be 428 lb. This weight estimate is based upon a number of assumptions that would need to be revised when applying this concept to an actual airplane design. For example, the weight savings that will result when there is no fan blade containment system, manufacturing limitations which may increase the weight where variable thicknesses was assumed, engine placement on the wing versus aft fuselage, etc.

1.0 Introduction

The Federal Aviation Administration (FAA) has been engaged in discussions of open-rotor turboprop engine aircraft safety regulations with airframe and engine manufacturers. There exists a concern that maintaining the current level of safety provided by the engine containment system, which provides mitigation at the airframe level, for the open-rotor concepts would result in a large weight penalty due to fuselage shielding protection for blade loss events. Unlike a typical engine configuration where blade loss is mitigated with fan case containment, with an open-rotor there is no containment structure, and therefore blade loss protection would need to be provided by the aircraft fuselage. By studying a representative

airframe and open-rotor engine configuration, and calculating the required shielding to prevent blade penetration, the weight penalty for continuing the current level of safety (i.e., no penetration by the blade) can be assessed. At the request of the FAA, the Naval Air Warfare Center (NAWC) China Lake had undertaken a parallel study based on a high wing configuration and a surrogate propeller blade geometry. (In their assessment, NAWC made use of the empirical Uncontained Engine Debris Damage Assessment Model (UEDDAM equation) to obtain a required shielding thickness (Ref. 1)). The FAA desired a more detailed finite element analysis, and requested that the present study be performed. The same geometric and operational parameters were used for both the NAWC study and this study to make a direct comparison between the results. A counter-rotating configuration was assumed and an appropriate rotational velocity was defined. A medium-size passenger aircraft served as the basis for the fuselage geometry.

Since new open-rotor designs will likely use composite fan blades and airframes, composite materials were utilized for this study. A triaxially-braided composite of TORAYCA T700S fibers and CYCOM PR520 toughened resin was selected. The braid architecture was composed of 24 k tows in the 0° direction and 12 k tows in the $\pm 60^\circ$ directions with the same fiber volume in each direction so that the in-plane stiffness properties were quasi-isotropic. This particular material and fiber architecture was selected for several reasons. First, due to the quasi-isotropic properties, each layer in the composite is identical, and delamination due to inter-ply property mismatch is minimized, resulting in good impact properties. Second, from a manufacturing point of view, this material is both practical and affordable. Lastly, considerable mechanical property and impact test data, as well as analytical material modeling results are available for this material (Refs. 2 to 8). The same braided composite system was used for both the notional blade and shielding structures. This material may not be optimal for a composite blade design, but its relatively high toughness provides for a conservative estimate of shielding requirements. Because of the test verification available for the material modeling, there is a relatively higher level of confidence in the analytical results than is typical for conceptual studies.

A trajectory study was undertaken to establish the blade impact analysis initial conditions, including blade orientation, with respect to the fuselage and blade velocity vector. A rotating blade was released from various engine rotor angular positions, and the velocity and orientation at fuselage contact were recorded. The position with the highest perpendicular impact velocity was defined as the worst-case and the corresponding orientation was identified. This worst-case orientation and velocity vector scenario was then used for the subsequent impact analysis. The trajectory study was also used to establish the areas where shielding would be required. Aerodynamic forces derived from the F31/A31 Open-rotor aerodynamic simulation study (Ref. 9) and applied to the present configuration were shown to cause a dispersion fore and aft of the blade rotational plane of less than the $\pm 3^\circ$ currently specified in the FAA regulations for disc burst evaluation. Thus, a conservative dispersion of $\pm 3^\circ$ was used to identify the area where shielding would be required in the present study.

Impact analysis was performed using the explicit integration finite element software, LS-DYNA (Ref. 10). This software is specifically designed for modeling highly non-linear behavior, including failure, both accurately and with computational efficiency. A series of analyses using the worst-case impact conditions and various thicknesses of shielding were performed. Using the results from these analyses, the required shielding thickness to prevent penetration was established.

2.0 Geometry

The FAA provided a set of parameters, which are a realistic representation of a prospective open-rotor engine and airframe design. The approximate dimensions and complex 3D geometry of the provided surrogate open-rotor blade are shown in Figures 1 and 2. Physical parameters of the released surrogate blade are shown in Table 1.



Figure 1.—Surrogate blade provided by the FAA.

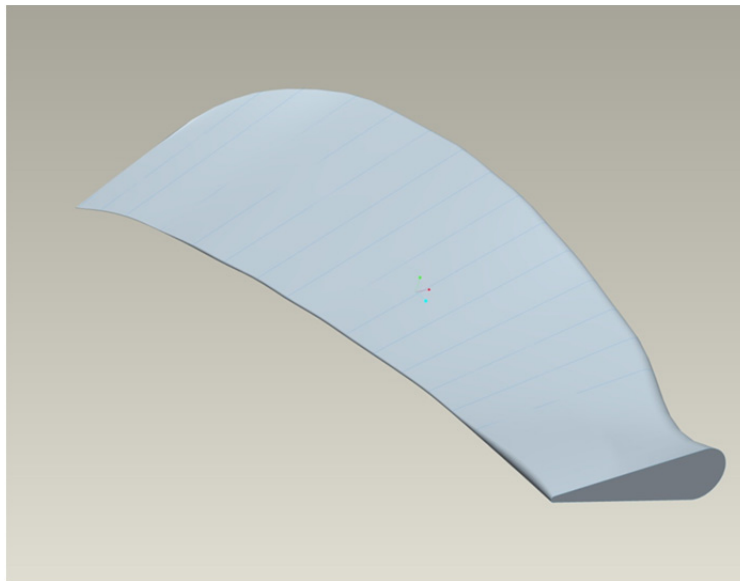


Figure 2.—Surrogate blade geometry.

TABLE 1.—SURROGATE BLADE
FRAGMENT PARAMETERS

Maximum width	12 in.
Length	41.28 in.
Maximum thickness	2 in.
Density	0.057 lb/in. ³
Weight	17 lb

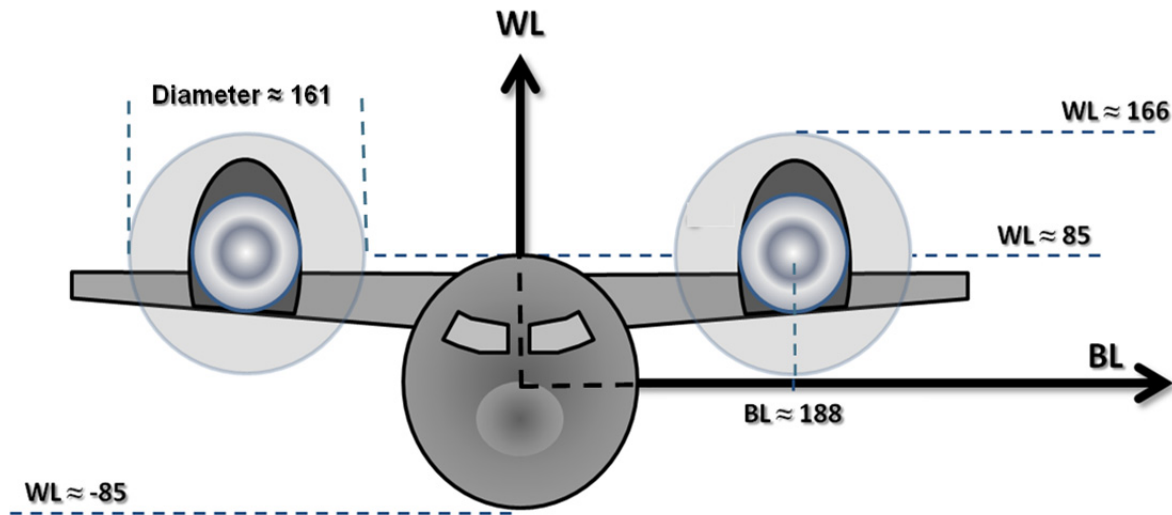


Figure 3.—High wing mounted open-rotor study airframe geometry.

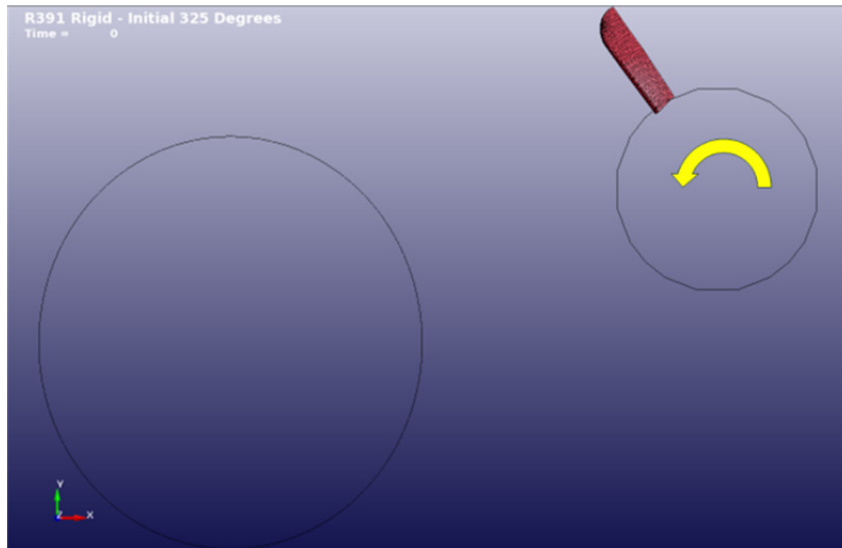
A medium-range, twin-engine, narrow-body jet airliner served as the basis for the notional open-rotor aircraft. The geometry assumptions, shown in Figure 3, were obtained from the FAA-directed, NAWC Open-Rotor Analysis (Ref. 11). The horizontal distance from the centerline of the fuselage to the centerline of the engine is approximately 188 in. (BL or Butt Line axis). The vertical distance from the centerline of the fuselage to the center line of the engine is approximately 85 in. (WL or Water Line axis). The diameter of the engine hub was assumed to be approximately 78.5 in., and with the length of each blade being approximately 41.28 in., the overall open-rotor engine diameter is approximately 161 in.

The selection of wing-mounted engines was a conservative assumption relative to aft-fuselage mounting, since the distance from the fuselage to the engine results in a larger area of shielding and additional weight. The high-wing configuration was chosen to expedite this study because of the availability of airframe modeling. This configuration does not address concerns of opposite engine damage, so an underwing or aft fuselage location for the engines may be required in an actual open-rotor design.

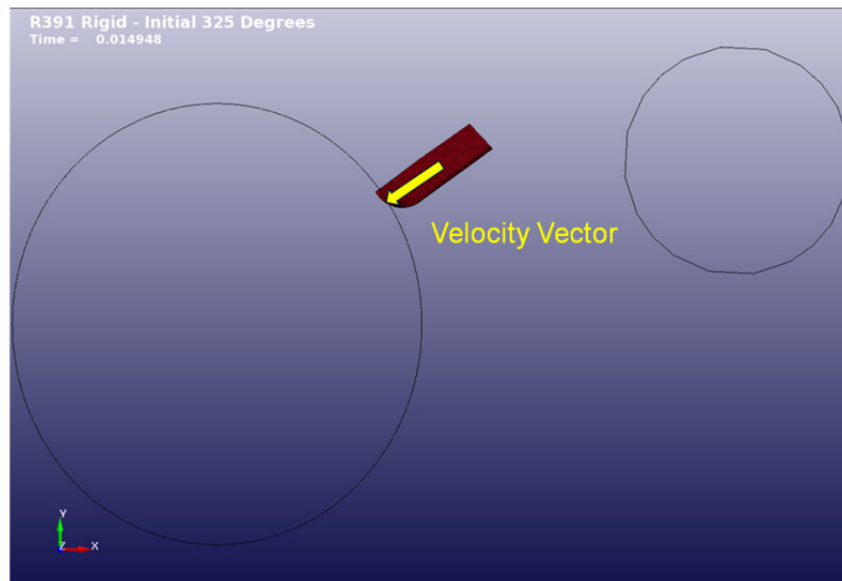
3.0 Initial Impact Conditions Trajectory Study

A trajectory study was conducted to determine the worst-case angle and velocity for the impact analysis. The results from the trajectory study were then used as initial conditions for the impact analysis. The blade impactor could then be placed close to the fuselage at the beginning of the impact analysis. Starting the impactor close to the fuselage minimizes the computational run times for the impact analyses.

A rotating blade was released from various angular positions on the engine, initially in 15° increments. The rotational velocity was 1,020 rev/min (106.8 rad/sec), and the tip speed of the blade at release was 718.6 ft/sec. The velocity and orientation of the blade at fuselage contact were recorded. Both front and aft rotor (counter-rotating) blade releases were assessed. The impact angle and velocity that leads to the highest perpendicular impact velocity were then used as initial conditions for the impact analysis. Smaller release angle increments were used to find the worst-case release was from an angle of 35° in the direction of rotation relative to vertical (Fig. 4(a)). This release position led to an impact velocity of 509.7 ft/sec perpendicular to the fuselage. The orientation of the blade was blade tip first, with the blade aligned with the velocity vector (Fig. 4(b)).



Figures 4(a).—Release location of the worst-case impact orientation.



Figures 4(b).—Impact location of the worst-case impact orientation.

Other impact conditions, or non-impact conditions when the blade misses the fuselage, are shown in Figures 5(a) to (f). These are classified by release position. The 15° and 60° release locations led to shallow angle impacts, while for the 0° and 75° release locations the blade missed impacting the fuselage. In each of these figures, the red bar signifies the release position of the blade.

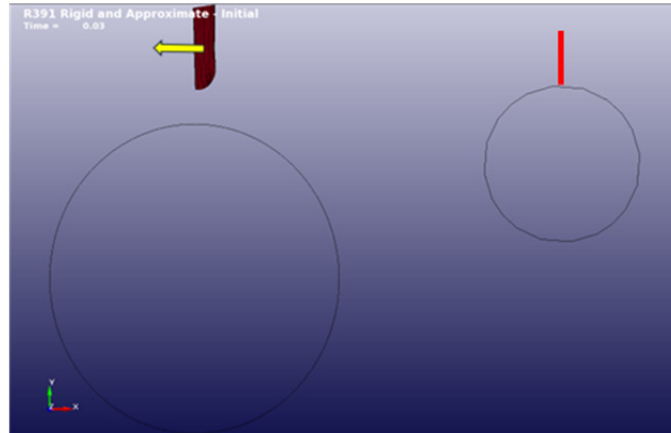


Figure 5(a).—0° initial position—missed fuselage.

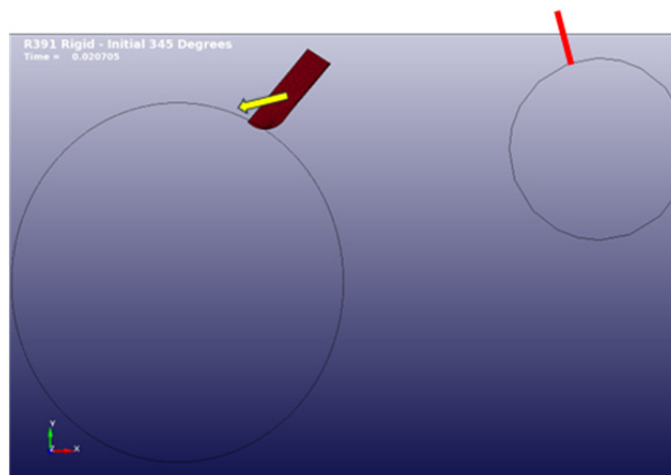


Figure 5(b).—15° initial position—contact location.

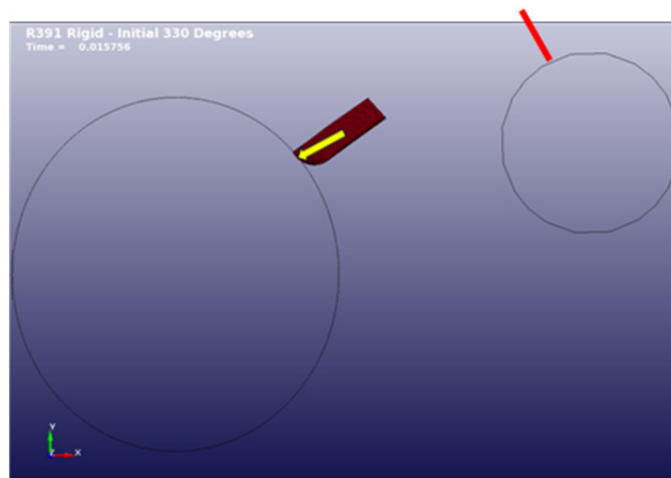


Figure 5(c).—30° initial position—contact location.

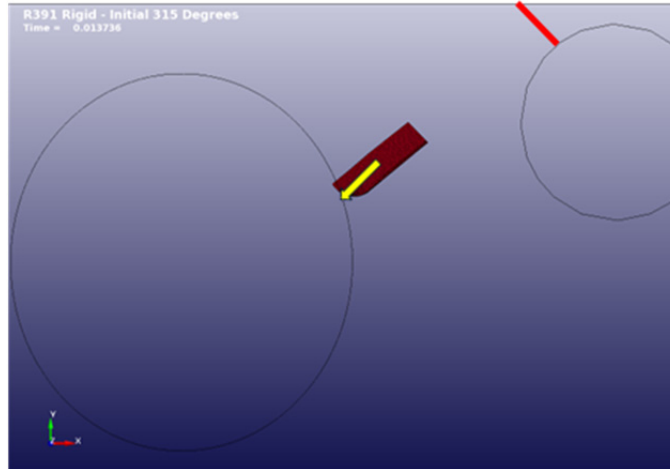


Figure 5(d).—45° initial position—contact location.

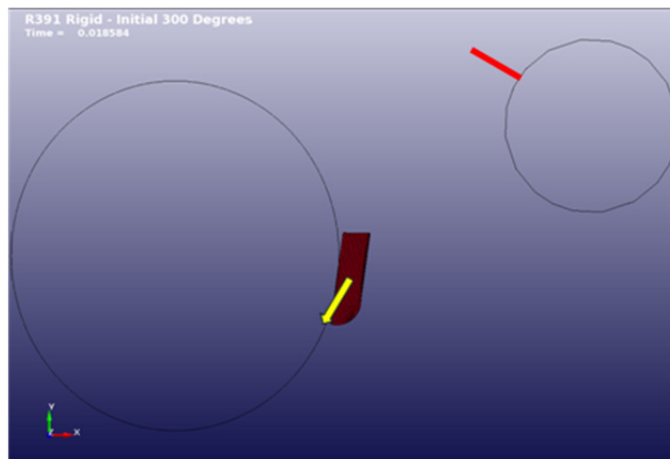


Figure 5(e).—60° initial position—contact location.

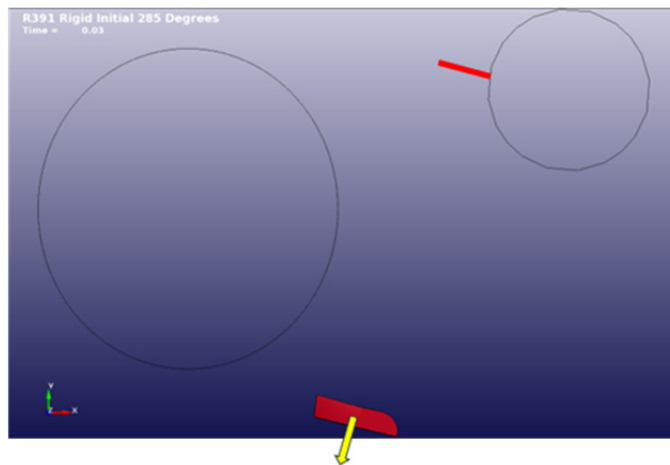


Figure 5(f).—75° initial position—missed fuselage.

Trajectory analysis was also run for a counter-rotating blade. Impact positions are shown in Figures 6(a) to (f), and release angle was also defined from a straight up blade in the direction of rotation. The release from the 180° position led to impact conditions very similar to the 35° worst-case release discussed in the preceding paragraph.

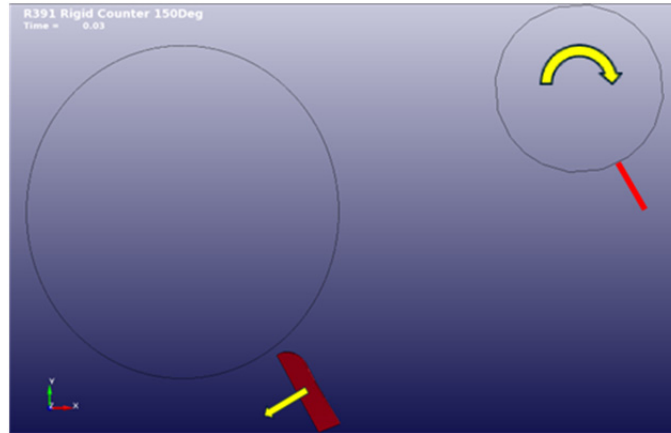


Figure 6(a).—150° initial position—missed fuselage.

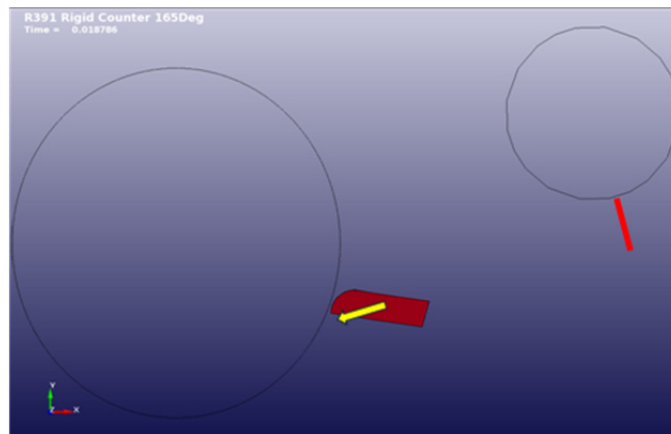


Figure 6(b).—165° initial position—contact location.

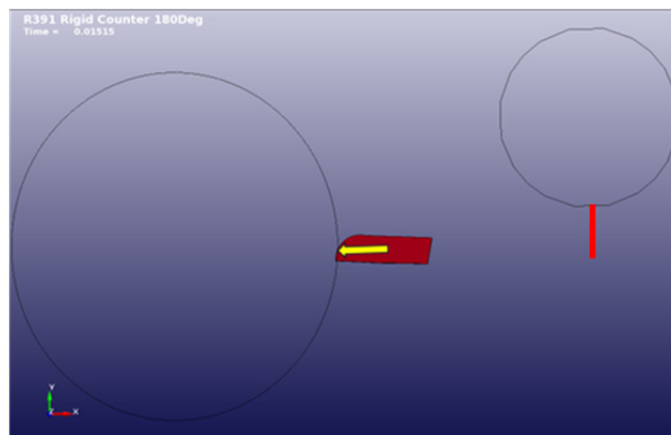


Figure 6(c).—180° initial position—contact location.

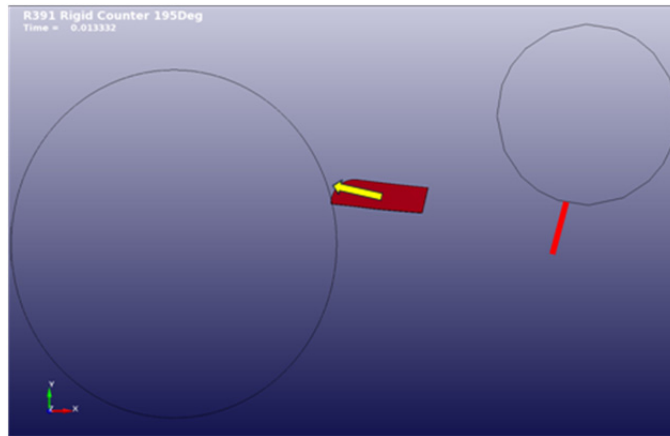


Figure 6(d).—195° initial position—contact location.

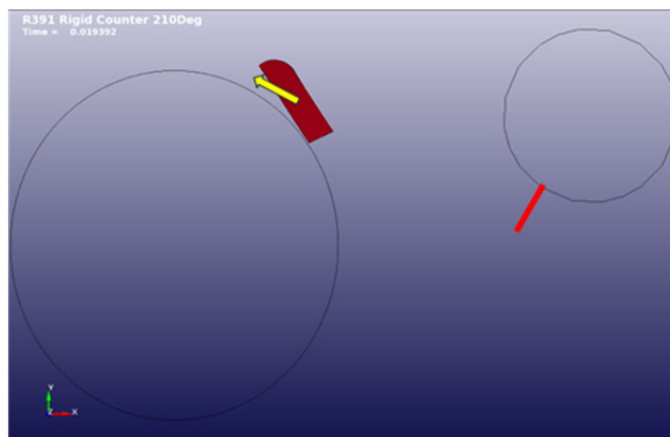


Figure 6(e).—210° initial position—contact location.

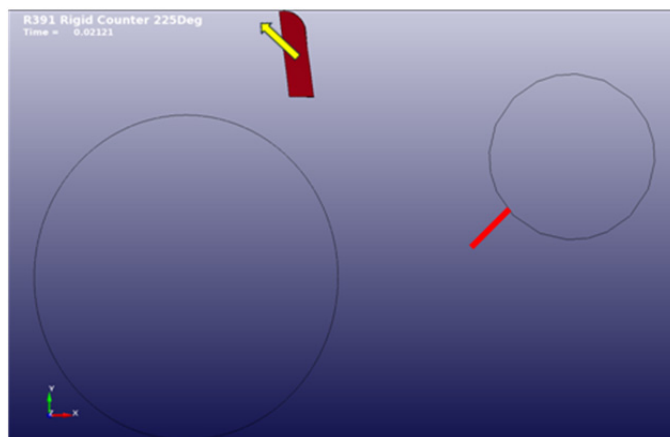


Figure 6(f).—225° initial position—missed fuselage.

Overall, approximately the lowest quarter of the fuselage is not impacted regardless of the release angle. Furthermore, sections on both the upper and lower portions of the fuselage are only contacted by shallow angle impacts. As a result, shielding thick enough to prevent penetration of the worst-case impact conditions is not required for all of the fuselage cross section. On this basis, variable thickness shielding will be used for the final shielding weight estimates.

4.0 Effect of Aerodynamic Forces on Blade Trajectory

After blade release, aerodynamic forces will affect the blade trajectory, and the location where the blade will impact the fuselage. Instead of the blade impacting somewhere in the rotation plane, aerodynamic forces will alter the trajectory, and cause the blade to impact either upstream or downstream from the rotation plane. This effect leads to a requirement to provide fuselage shielding forward and aft of the blade rotation plane.

A simple study was performed to determine the magnitude of force required to alter the blade trajectory from the rotation plane. Varying body forces were applied to a blade released from the 35° initial position (release position for worst-case impact conditions.) The force was applied perpendicular to the plane of blade rotation and in the direction of the aircraft flight, and it did not vary in time. The resulting displacement at the point of impact was recorded for each out of plane force magnitude (Fig. 7), and a dispersion angle was calculated. The distance that the blade traveled in the worst-case blade release was 119.43 in., and the angle was calculated using this value. The out-of-rotation plane forces required to produce dispersed angles up to $\pm 15^\circ$ are shown in Figure 8. When the blade is released with no out-of-rotation plane forces, it travels forward 2.89 in. due to the initial difference between the blade's center of gravity and its center of rotation. As a result, both the displacements and angles shown in Figures 7 and 8 are slightly off center.

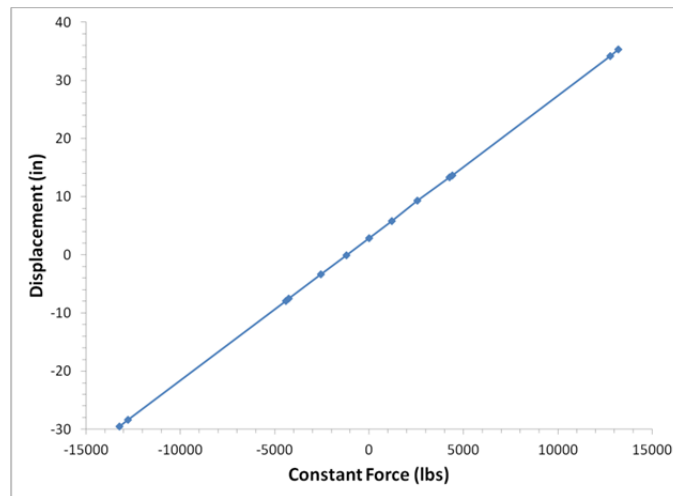


Figure 7.—Out-of-plane displacement versus force.

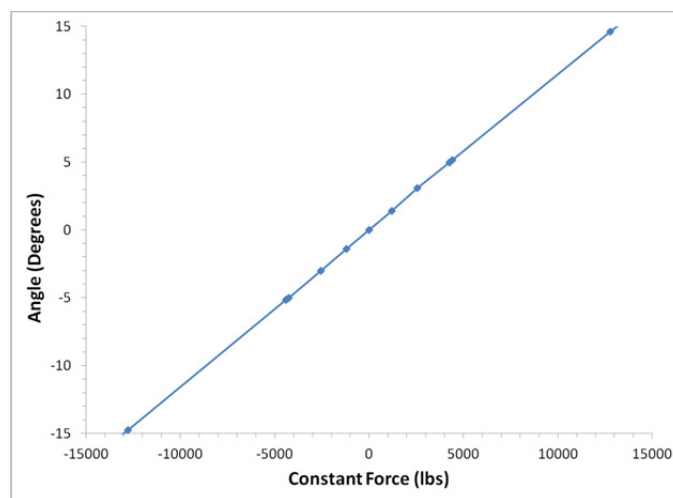


Figure 8.—Out-of-plane dispersion angle versus force.

A joint effort between NASA and GE Aviation had previously been conducted to investigate the aerodynamic performance of modern blade designs (Ref. 9). A part of this effort has been the assessment of tools for predicting the aerodynamic performance of open-rotors. For that purpose a baseline, vintage 1990s, blade design called the historical blade set (also known as F31/A31) was selected for evaluating various prediction tools. F31/A31 has 12 front rotor fan blades and 10 aft rotor fan blades.

Comprehensive aerodynamic data sets were acquired in NASA Glenn Research Center wind tunnels for a ~25.6 in. diameter sub-scale model of this blade set. The test campaign included both low speed testing in the NASA 9- by 15-ft wind tunnel to investigate the aero/acoustic performance at operating conditions in the approach to takeoff range as well as high speed testing in the NASA 8- by 6-ft wind tunnel to analyze the aerodynamic performance in the speed range between climb and cruise conditions. The difference in total thrust between the analysis and the test data was less than 5 percent. The analytical forces of the individual blades can be compared to the results in Figures 7 and 8 to estimate the dispersion, which will occur in a typical open-rotor blade loss. However, the F31/A31 blade is smaller than blade used in this study, so the aerodynamic forces from the F31/A31 analysis were proportionally scaled upward to account for the larger area of the study blade.

The length of the F31/A31 forward blade is 7.673 in., while the study blade length is 41.28 in., and the base chord length of the F31/A31 forward blade is 2.576 in., while the study blade base chord length is 12 in., leading to a scale factor for the forward blade of 25.06. The length of the F31/A31 aft blade was 7.618 in. and its width was 2.773 in., leading to a scale factor for the aft blade of 23.45. The blade thrust levels scaled up from the F31/A31 size blade to the study size blade are shown in Table 2. The thrust levels presented are for cruise for nominal operations at an altitude of 30000 ft.

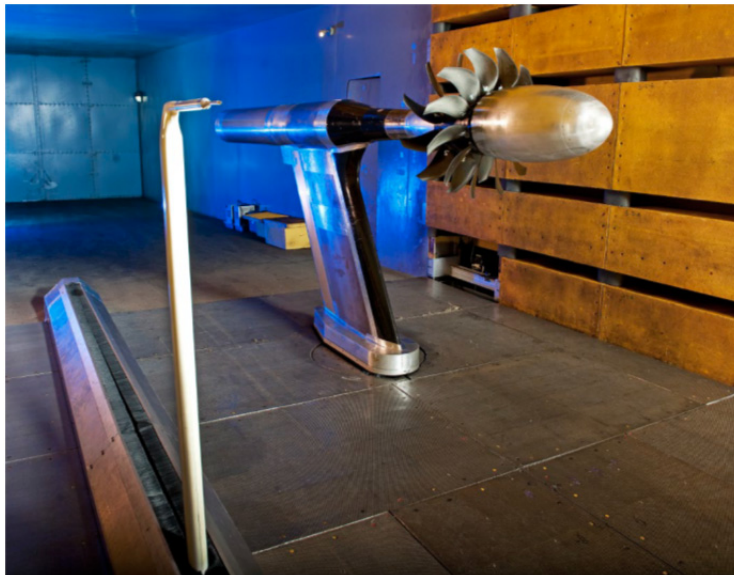


Figure 9.—Model scale F31/A31 historical baseline blade set.

TABLE 2.—AERODYNAMIC FORCES ON THE STUDY OPEN-ROTOR BLADE

Aerodynamic forces	Forward rotor, lb	Aft rotor, lb
Take-off	606	733
Cruise	269	461

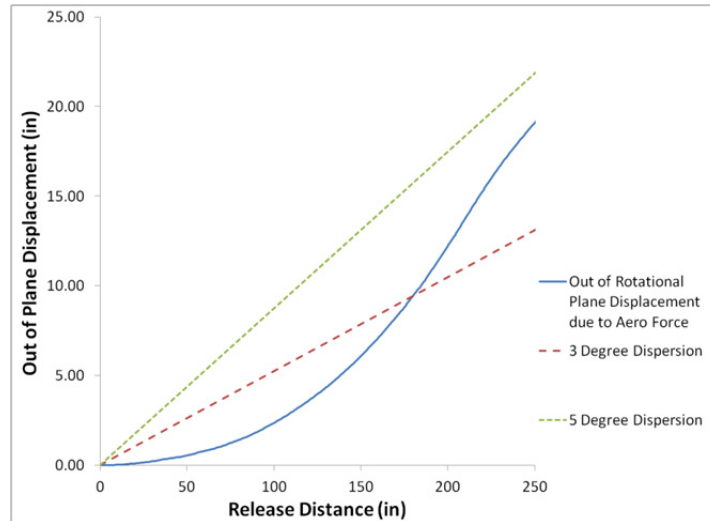


Figure 10.—Out-of-plane displacement due to aerodynamic forces.

Both the cruise and the take-off thrust force acts in the direction of flight, causing a released blade to travel forward. However, because of the large blade mass and initial velocity, a very large force is required to deflect the blade significantly out of its initial plane of rotation. For example, comparing the larger take-off forward and aft aerodynamic forces from Table 2 (733 and 606 lb) to the results in Figure 8 yields dispersion angles of less than 1°. Comparing these same aerodynamic forces to the results in Figure 7 yields a forward displacement of ~1.5 in. for the forward rotor and ~1.8 in. for the aft rotor.

The further the engine is located away from the fuselage, the greater the dispersion angle would be after a blade loss. With a constant aerodynamic force the blade would not follow a linear trajectory. Figure 10 shows a plot of the blade out of plane displacement as a function of the distance between the blade tip at the time of release, and the location where the blade impacts the fuselage. The results in Figure 10 show that for the aft blade to reach a 3° dispersion angle, under the take-off aerodynamic force, a release distance of nearly 180 in. would be required, which is not the case for the present aircraft configuration. As discussed above, the worst-case scenario release distance in this study is 119.43 in.

Regardless of the distance from the blade release position to the fuselage, the shielding can be centered at the probable impact location, and not at the blade's release location. Since the aerodynamic force will consistently move the blade forward, the shielding can be placed forward of the initial plane of rotation, according to the engine's distance from the fuselage. As a result, other potential open-rotor configurations, leading to alternate release geometries, would not necessarily require any additional shielding area.

As an additional example demonstrating that the aerodynamic forces are small compared to what would cause significant blade dispersion, a simple drag force calculation was made. Conservatively, using the length and the width of blade and calculating the blade area as if it were a rectangle, gives a blade frontal area of 495.36 in.². Using an air density of 1.37E-5 lb/in.³ (35,000 ft altitude), and assuming an aircraft velocity of 9680 in./sec (550 mph), a drag coefficient of 1.2 (rectangular plate with a length/width = 5), and that the rectangular plate is perpendicular to the air flow direction, the drag force is,

$$\text{Drag Force} = \frac{1}{2} \rho V^2 A C_D \quad (1)$$

This equation yields a drag force of ~990 lb, significantly below the force level of ~2550 lb which would cause a 3° dispersion. The drag force calculated in this simple example should not be compared to the actual aerodynamic forces presented in the previous paragraphs, and is only presented to demonstrate the improbability of aerodynamic forces significantly affecting a released blade's trajectory.

5.0 Material Modeling

Extensive mechanical property and ballistic impact tests have been conducted by the GRC Impact Dynamics Group for the T700S/PR520 braided composite system used in this study (Refs. 2 to 5). The mechanical property test results, which were used to populate the LS-DYNA model of the T700S/PR520, are shown in Table 3. The reference for each of these parameters is provided in the table. The average properties from these reports were used and the associated uncertainties were reported in the references. The out of plane shear modulus was assumed to be that of the epoxy alone, and was calculated using test measurements of the epoxy's Young's Modulus and Hooke's law. In between the braided layers of T700S, shear loading would be resisted by the epoxy alone. As a result, the shear modulus of the epoxy is representative of the composite out of plane shear modulus, and represents the minimum value which it could be. The transverse tensile strength and its associated strain are set equal to the longitudinal values. This is consistent with the results shown by Kohlman (Ref. 4), who demonstrated that standard composite test specimen designs do not properly account for edge effects in braided composites, and so underestimate the value of transverse tensile strength. In addition, the architecture of this braided composite is consistent with the expectation of similar longitudinal and transverse tensile strength properties.

TABLE 3.—MATERIAL PROPERTIES USED IN THE T700S/PR520 MODELING

Material property	Value	Source
Density	0.0645 lb/in. ³	Ref. 8
Young's modulus—longitudinal	6.904E+06 lb/in. ²	Ref. 2
Young's modulus—transverse	6.092E+06 lb/in. ²	Ref. 2
Poisson's ratio	0.31	Ref. 3
Shear modulus—in-plane	5.062E+06 lb/in. ²	Ref. 2
Shear modulus—out-of-plane	2.214E+05 lb/in. ²	Ref. 2
Strain at longitudinal compressive strength	0.018	Ref. 3
Strain at longitudinal tensile strength	0.021	Ref. 4
Strain at transverse compressive strength	0.012	Ref. 3
Strain at transverse tensile strength	0.021	Ref. 4
Strain at shear strength	0.011	Ref. 3
Longitudinal compressive strength	5.329E+04 lb/in. ²	Ref. 4
Longitudinal tensile strength	1.418E+05 lb/in. ²	Ref. 4
Transverse compressive strength	4.663E+04 lb/in. ²	Ref. 4
Transverse tensile strength	1.418E+05 lb/in. ²	Ref. 4
Shear strength	4.596E+04 lb/in. ²	Ref. 4

Strain rate dependent testing results for this braided composite, in tension, are currently only available at three relatively low strain rates (Ref. 4). Since the impact event produces higher strain rates than what existing data covers, the measured strain rate sensitivity was extrapolated to the required higher strain rates for the present application. The available data and the extrapolated results are shown in Figure 11. The strength increase (~17 percent increase at 1,000 1/sec over static) due to the extrapolated rate sensitivity is consistent with that observed in the single high strain rate test conducted on this braided composite in compression (Ref. 5).

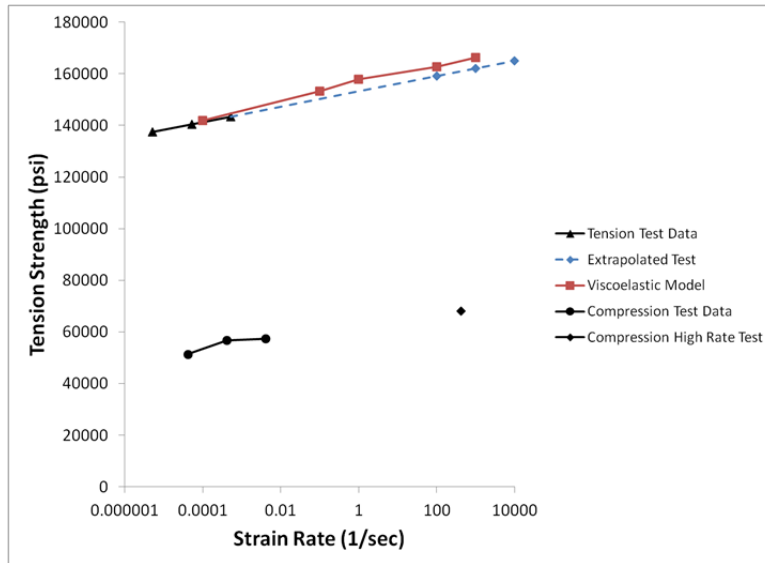


Figure 11.—Strain rate sensitivity of T700S/PR520.

TABLE 4.—PRONY SERIES FOR MODELING RATE EFFECTS

Shear relaxation term	Shear decay constant
3.0E+05	1.0
1.5E+05	10.0
1.5E+05	1000.0
1.5E+05	100000.0

The most commonly used, and reliable, material models in LS-DYNA (Ref. 10) for composite shell elements are Laminated Composite Fabric (Mat 58) and the Rate Sensitive Composite Fabric (Mat 158). Both of these material models are based on Schweizerhof's (Ref. 12) implementation of Matzenmiller's (Ref. 13) theoretical approach. This approach is a continuum damage model, and includes damage parameters which control the non-linearity of the stress-strain curve. In Schweizerhof's implementation, there are three damage parameters (one for each of the two orthogonal directions, and one for shear), which are initially set to 0. Each integration layer in the composite has its own set of damage parameters. As strain increases, and one of the parameters in an individual shell integration layer reaches 1, failure occurs, and the element can no longer take load.

Several different approaches may be taken in the use of Mat 158 to model composites (Refs. 6 to 8). The modeling approach used with Mat 158 in this study was the homogeneous approach, where a single set of input parameters describes the composite material. The input parameters for the Rate Sensitive Composite Fabric material model in LS-DYNA were created from the information in Table 3 and Figure 11. The failure surface type was defined as faceted (FS = -1). All of the factors to determine the minimum stress limit after stress maximum (SLIMs) were set to 1.

In the Rate Sensitive Composite Fabric model (Ref. 10), strain rate effects are included by the addition of a viscous stress tensor, which is based on an isotropic Maxwell model with terms in a Prony series expansion. The terms are superimposed on the rate independent stress tensor of the composite fabric, and so are quasi-isotropic. Since the braided composite system used in this study is also quasi-isotropic, this viscoelastic representation of strain rate effects is acceptable. The terms are defined as a shear relaxation modulus and a shear decay constant, and must be determined by analytical trial and error. The terms used in this study are shown in Table 4, and the match to the extrapolated strain rate sensitivity is shown in Figure 11.

The element erosion criteria associated with the composite material model was calibrated by comparisons to a series of ballistic impact tests (Ref. 5). In these tests, a spherical nosed cylindrical aluminum projectile with a spherical front face was shot at 0.125 in. thick T700S/PR520 composite plate. The projectile was semi-hollow, with a radius of 0.9975 in. and a wall thickness of 0.03 in. in the cylindrical section, and with a spherical nose front face radius of 1.5 in. thickened to 0.25 in. The projectile's overall length was 1.947 in., and a cross-section of the projectile is shown in Figure 12. The braided composite plate was 12.0 by 12.0 in., with the plate being held in a fixture with a 10 in. diameter aperture. The results of these ballistic tests are shown in Figure 13. A ballistic limit (highest contained velocity) of 540 ft/sec was selected to use in the material model correlation. There is a small amount of scatter in the data, with two tests using material from Plate 7 being penetrated at slightly lower velocities than one that was contained.

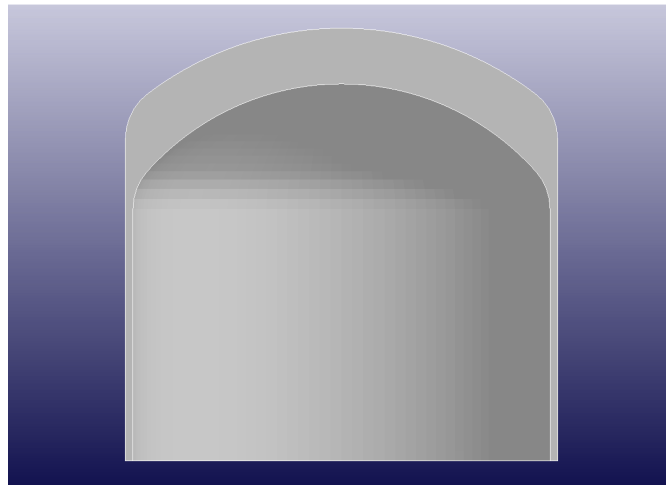


Figure 12.—Projectile cross-section.

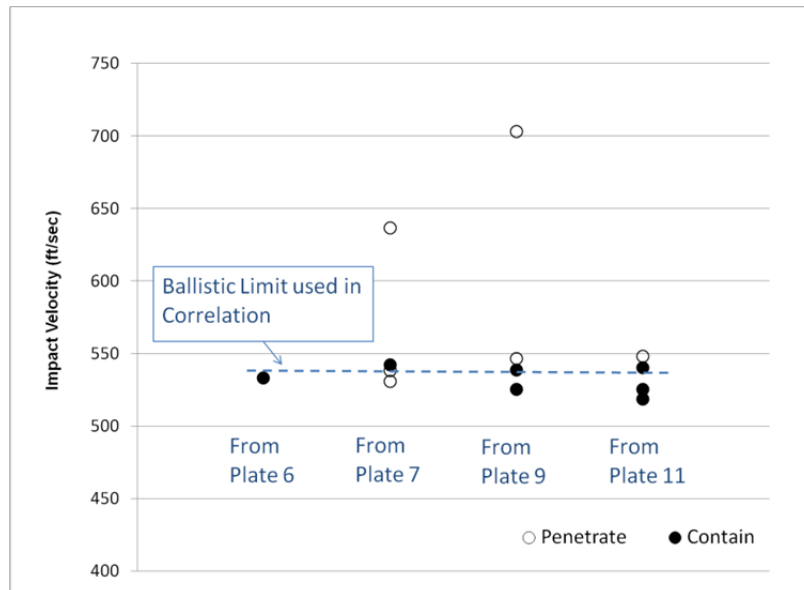


Figure 13.—Ballistic impact test results on T700S/PR520 composite plates.

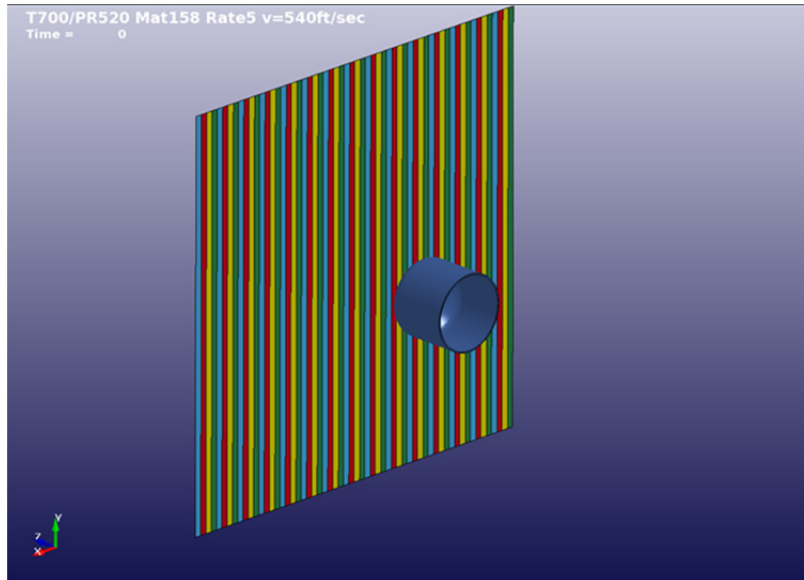


Figure 14.—Finite element model of ballistic impact test.

Finite element representations of the projectile and target were created, as shown in Figure 14, using a mesh size in the composite plate of 0.2 by 0.2 in. Separate analysis was conducted at both the 540 and 550 ft/sec projectile initial conditions. The element erosion criteria were then adjusted to match a highest contained velocity of 540 fps, while simultaneously matching the uncontained tests which occurred at 550 fps. The Add Erosion feature in LS-DYNA was used so that the compression and tension rupture properties could appropriately be specified separately. The final strains for element erosion were as follows; the minimum principal strain was -14.4 percent, the maximum principle strain was 14.7 percent, and the shear strain to failure was 13.7 percent. The results from the validation analyses are shown in Figures 15(a) and (b). Some element erosion is seen in Figure 15(a), similar to results of the 540 ft/sec impact tests. In Figure 15(b), the element erosion extends beyond the dimensions of the projectile, similar to the slightly higher 550 ft/sec impact tests.

As is typical, these element erosion strains were not the same as the mechanical property test derived strain to failure values shown in Table 3. In finite element analysis of failure, there is a mesh size dependency of strain to failure due to localization, preventing the direct use of mechanical property data to set the erosion criteria (Ref. 14). In addition, under impact conditions composites can exhibit a higher strain to failure than what is observed in mechanical property tests. This higher failure strain is most likely due to the complex local through-thickness deformation and stress state in the fibers when the material is subject to impact by a finite sized projectile. The material strength is unaffected by the higher element erosion strain.

The interior of the surrogate blade consists of a foam core. For this study, a low-density, closed-cell foam, identified as PDL, was used for the blade core. (PDL was an acronym for the (since defunct) Polymer Development Laboratory, an early supplier). PDL was selected because a validated foam material model was available from the Space Shuttle Program (Ref. 15). A previously created stainless steel material model was used for the metallic leading edge guard (Ref. 16).

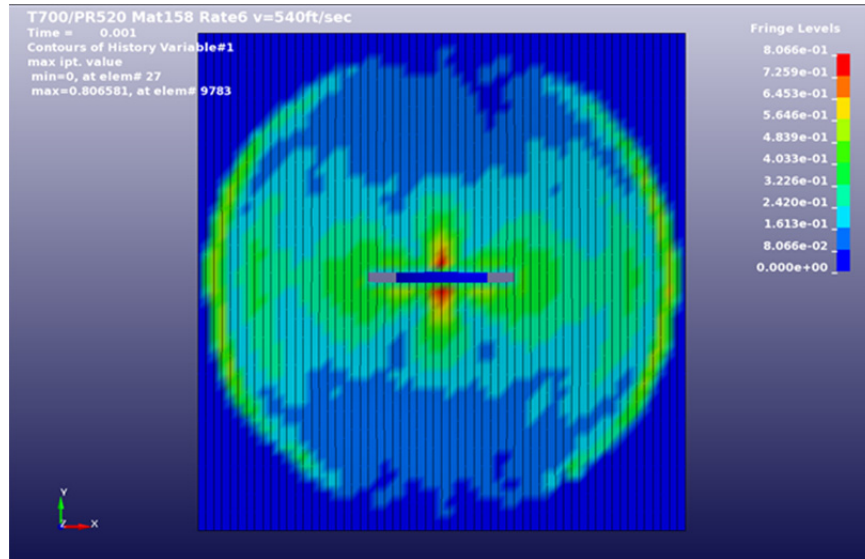


Figure 15(a).—540 ft/sec impact analysis.

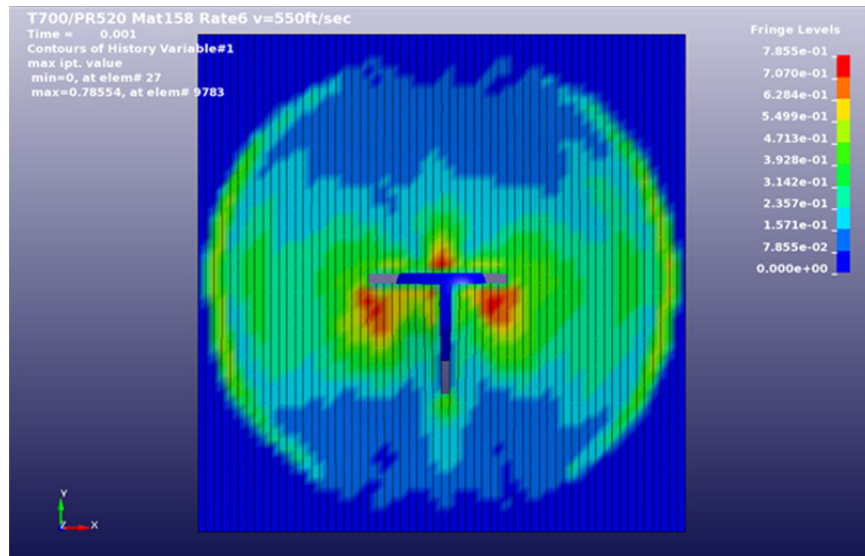
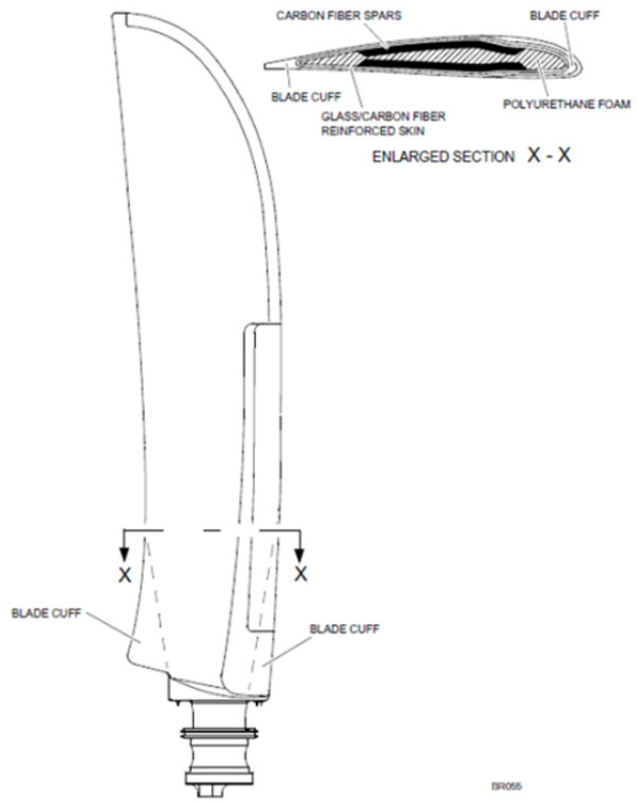


Figure 15(b).—550 ft/sec impact analysis.

6.0 Finite Element Discretization

A finite element mesh was created from the outer surface blade geometry. Since only the outer surface was available, and detailed drawings and geometry files of the surrogate blade interior were not available, the internal structure used for the finite element model was approximated, and does not represent an actual blade. Nevertheless, an attempt was made to adhere as close as possible to the surrogate blade during the finite element model creation, including a foam core and a composite shell and spar, as shown in Figure 16. The foam core of solid elements was covered by a set of shell elements representing the braided composites as shown in Figure 17. In this figure the differing colors represent sections with differing shell element thicknesses. For all shell elements, the node locations were defined to be the top surface of the element. By defining the nodes this way, correct blade thicknesses and center of inertias were properly defined. The same nominal mesh size (0.2 in.) used in the correlation and validation analysis was maintained for this study. Element sizes deviate from the nominal 0.2 in. locally due to the complex blade geometry.



Typical Blade Cuff

Figure 16.—Surrogate blade schematic.

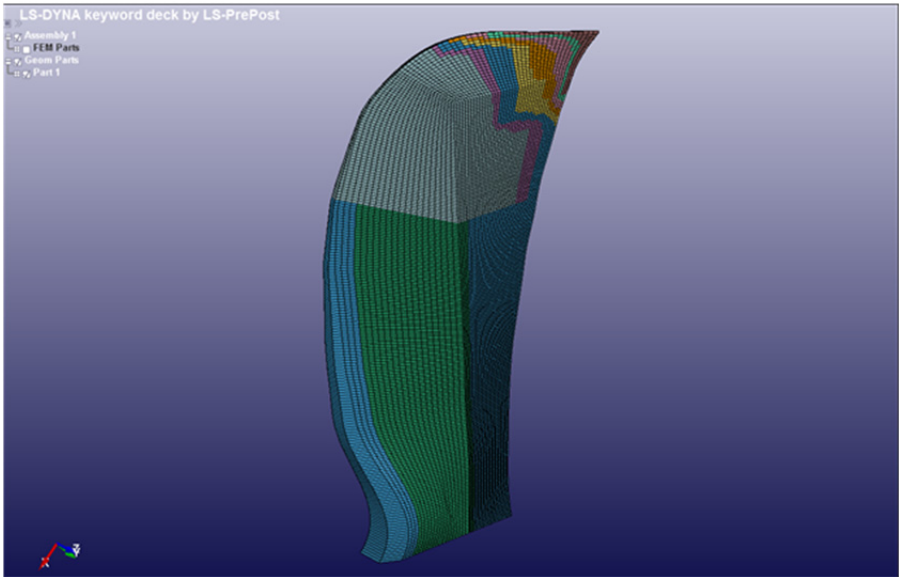


Figure 17.—Shell elements covering foam core of blade finite element model.

Thicknesses of the shell elements were decreased near the blade tip where the blade becomes thin, as shown in Figure 18. In this figure, the different fringe level colors represent the different shell element thicknesses. Near the end of the blade, the shell element thicknesses were set to be one half the thickness of the solid composite blade so that the combined thicknesses of the two shell element layers equaled the actual thickness of the blade. Thicknesses were obtained from the provided geometry. The two faces of shell elements were tied together with a rigid constraint so that the total thickness equaled the actual total thickness of the blade. In Figure 19, the two layers of shell elements near the blade tip are shown, with the straight yellow lines between these layers displaying the rigid constraints.

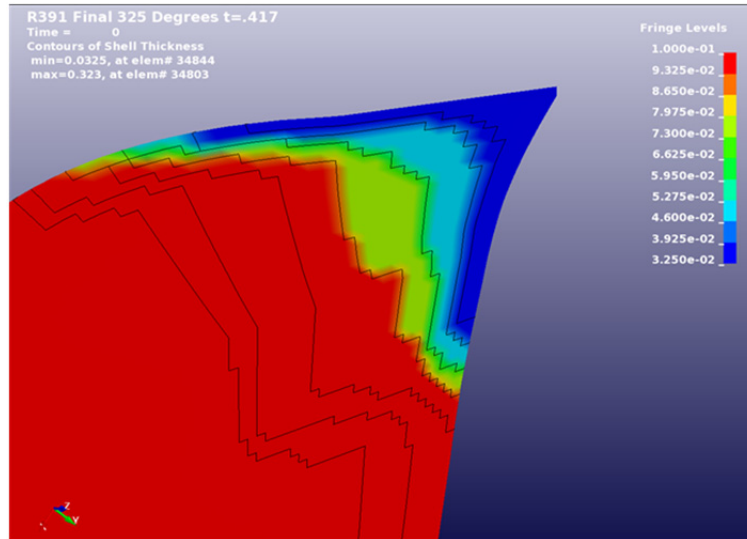


Figure 18.—Blade tip shell element thicknesses.

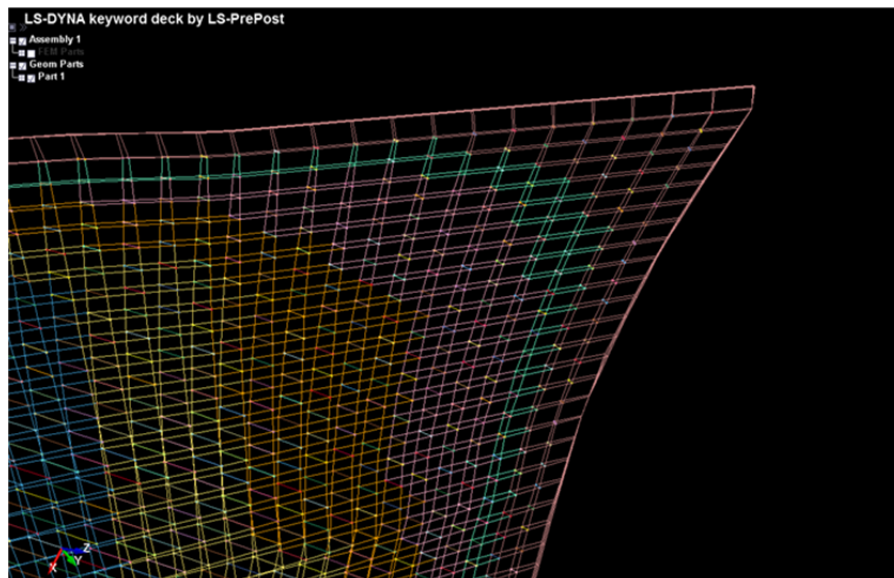


Figure 19.—Blade tip rigid constraints.

The shell thickness of the center section was increased in order to represent the blade spars. The spar thickness was estimated from the schematic shown in Figure 16. The spar thickness was set to 0.323 in., as shown in Figure 20. As in Figure 18, the different fringe level colors represent the different shell element thicknesses. The shell thickness in the remaining portions of the blade (other than the tip and the spar) was set to 0.104 in. This thickness was set so that the total weight of the blade matched the target weight of 17 lb. The center of gravity of the blade is ~17.5 in. from its base, and ~8.2 in. from the leading edge of the blade.

The foam core extends from the base of the blade out approximately 2/3 of the surrogate blade length. As a result, the solid foam elements representing the foam core were only included in the 2/3 region, as shown in Figure 21. This corresponds approximately to the region of the foam core in the actual blade.

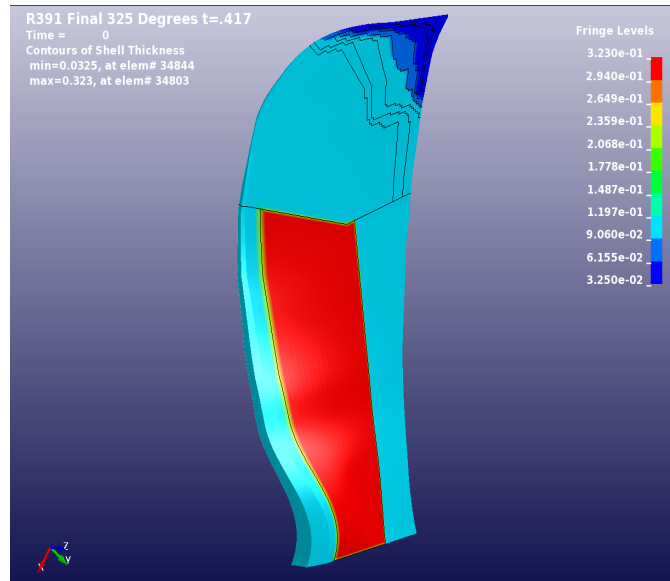


Figure 20.—Blade shell element thicknesses.

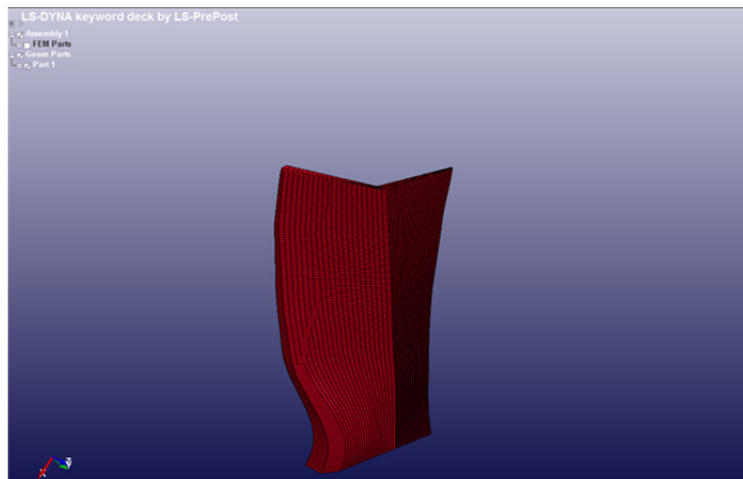


Figure 21.—Foam core solid elements.

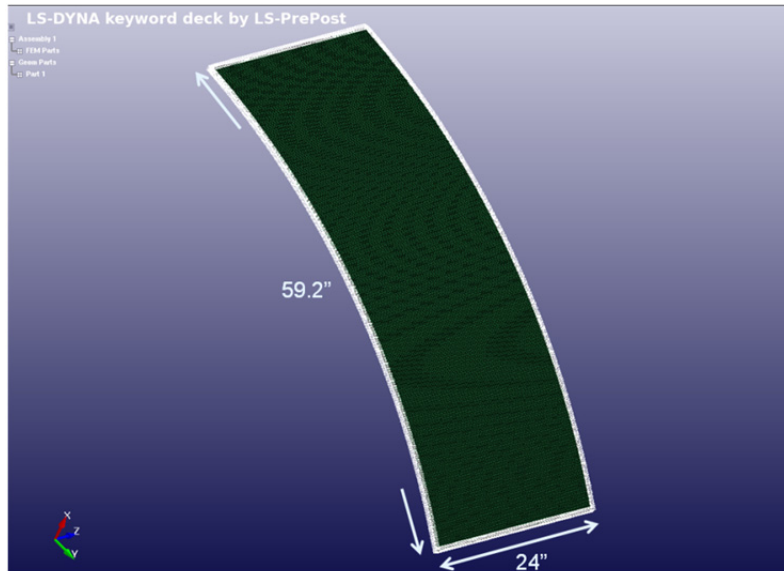


Figure 22.—Fuselage shielding finite element mesh.

A metallic leading edge guard, which some composite blades include to protect against nominal foreign object damage, was included. The leading edge guard was modeled as thin (0.005 in.) shell elements extending approximately 1 in. wide, on both sides of the blade.

The geometry of the study fuselage was based upon that of a medium-size airliner, with an elliptical shape and a major axis (height) of 157.87 in. and a minor axis (width) of 148 in. The same mesh size (0.2 in.) used in the material model impact analysis correlation and validation was used for the fuselage shielding mesh. This consistency is important for the validity of the onset of element erosion prediction. In order to reduce run times, only a $\sim 45^\circ$ (~ 59.2 in. arc length) of the fuselage shielding was included in the impact analysis, as shown in Figure 22. The fuselage shielding was 24 in. wide. Simply supported boundary conditions were enforced at the edges of the shielding.

7.0 Impact Analysis Results

The impact analysis was conducted using LS-DYNA. All impact analysis was conducted consistent with the modeling guidelines of the LS-DYNA Aerospace Working Group (Ref. 14). (For example, contact and hourglass energies were tracked and were at acceptable levels.) However, several uncertainties in the analysis remain. One uncertainty is that the initial impact of the relatively sharp composite blade tip could cause different failure modes than the blunt aluminum projectile used to develop the composite material model. Another remaining uncertainty is the current lack of a system level impact validation test closely resembling the present application that could be used to anchor the numerical results. Experience with these complex types of analysis has shown that physical testing is usually required to provide a higher level of confidence in the numerical results. For the present study, these uncertainties were considered to be acceptable.

As mentioned above, the initial conditions of impact velocity and blade orientation for the impact simulation were obtained from the trajectory study. This initial position is shown in Figure 23. As stated previously, the initial impact velocity is 509.7 ft/sec perpendicular to the fuselage skin at the impact location. The orientation of the blade was blade tip first; with the velocity vector pointed straight in. The blade also has an initial rotational velocity.

Several fuselage thicknesses less than 0.458 in. were analyzed and were found to provide inadequate shielding to prevent blade penetration. For shielding with a thickness of .458 in. (22 composite layers) the blade fails the fuselage surface but does not penetrate into the cabin. Just after initial contact, the blade tip elements fail while the fuselage is stressed below its failure limit. As the rest of the blade continues traveling toward the fuselage, the spar contacts the fuselage causing the shielding to fail. The spar, which is stronger and more massive than the blade tip, is what fails the shielding, as shown in Figure 24. Failure is identified by the element erosion that can be seen in the shielding. In this figure, the fringe color shows the maximum value of the damage parameter (which was discussed in Section 5.0) from any of the composite layers.

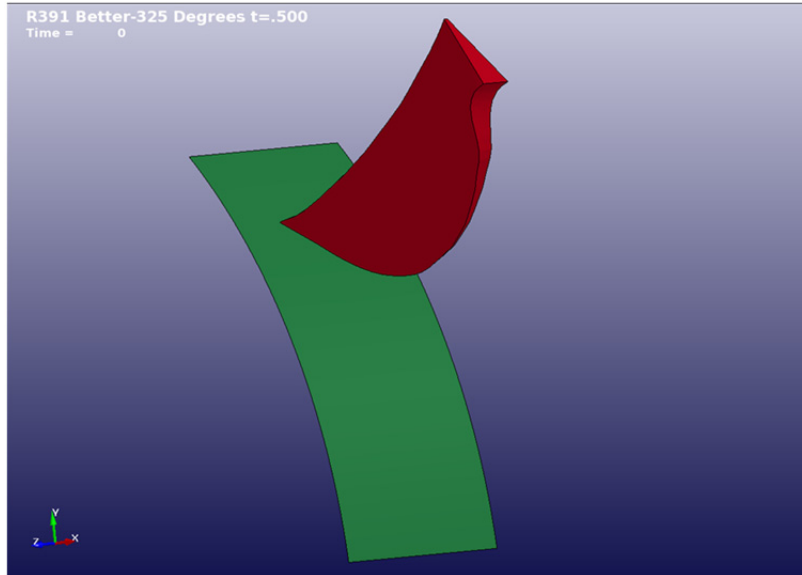


Figure 23.—Impact analysis initial position.

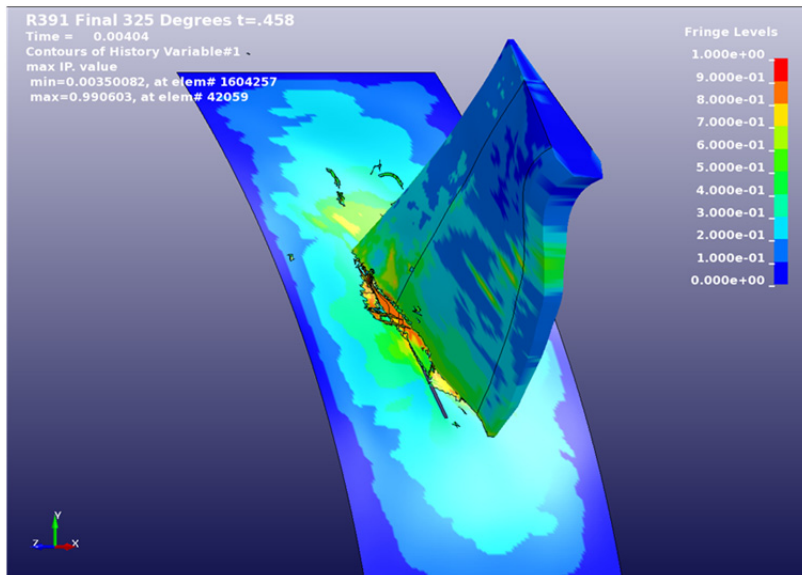


Figure 24.—Shielding failure with a 0.458 in. thickness.

When the thickness of the shielding was increased to 0.500 in. (24 composite layers), the fuselage shielding remained intact, with no breach of the skin and no element erosion, as shown in Figures 25(a) and (b). Both damage parameters 1 and 2 are shown in Figures 25(a) and (b), respectively, with damage parameter 1 being in the element plane of the circumferential (long) direction of the shielding, and damage parameter 2 being in the width (short) direction. As in Figure 24, the fringe color shows the maximum value of the damage parameter from any of the composite layers. A contour of deflections at the time of maximum deflection is shown in Figure 26. The maximum deflection was 1.533 in., and the time history of the deflection at the node where this occurred is shown in Figure 27. No attempt was made to further refine the required thickness calculations beyond the 0.458 in. that failed, and the 0.500 in. that prevented penetration.

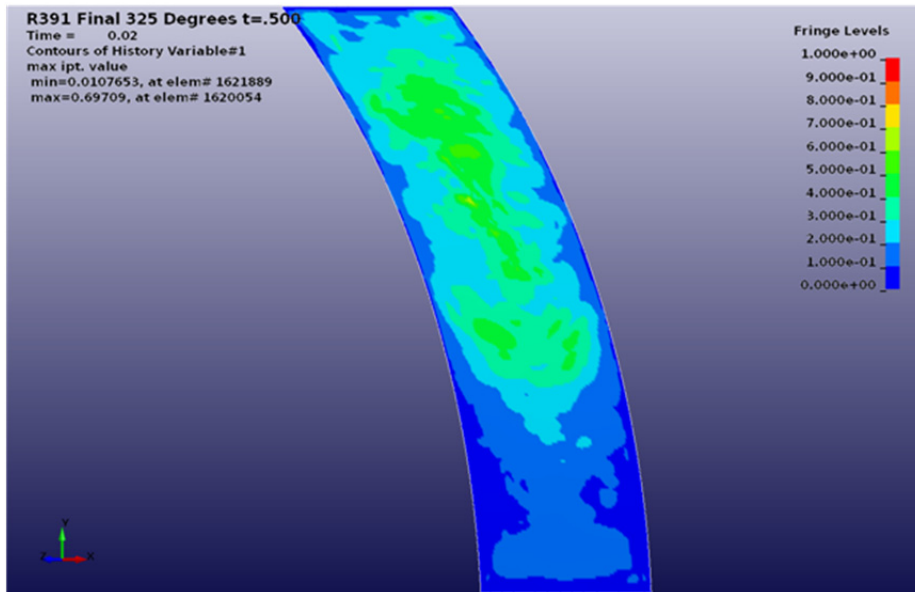


Figure 25(a).—Shielding containment with a 0.500 in. thickness, damage parameter 1.

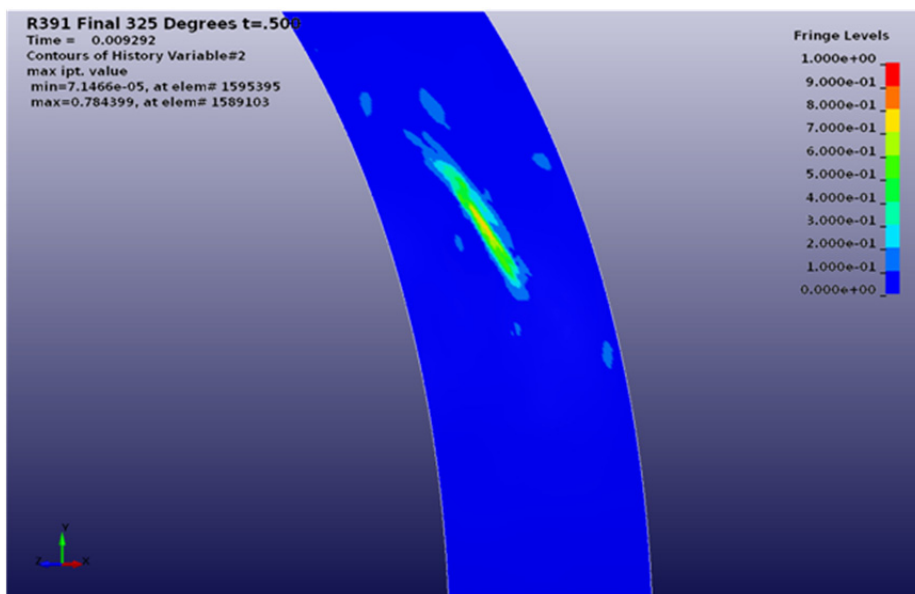


Figure 25(b).—Shielding containment with a 0.500 in. thickness, damage parameter 2.

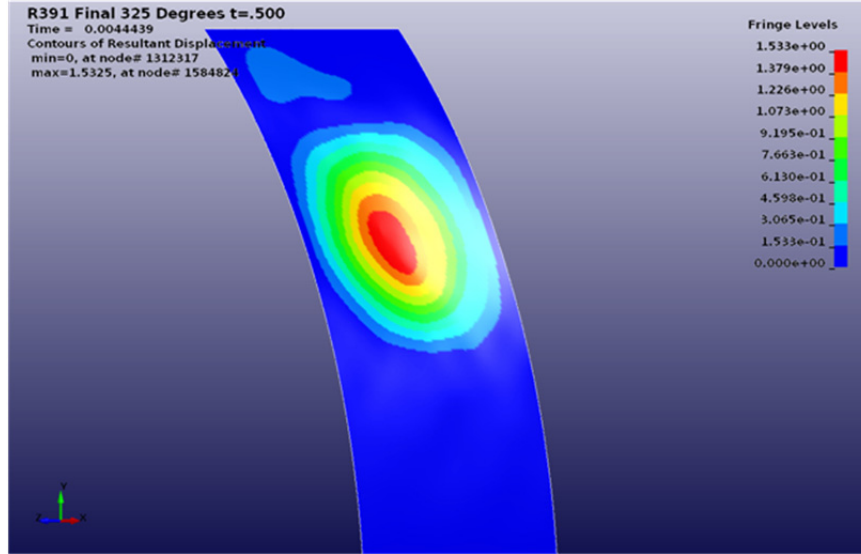


Figure 26.—Maximum displacement with a shielding thickness of 0.500 in.

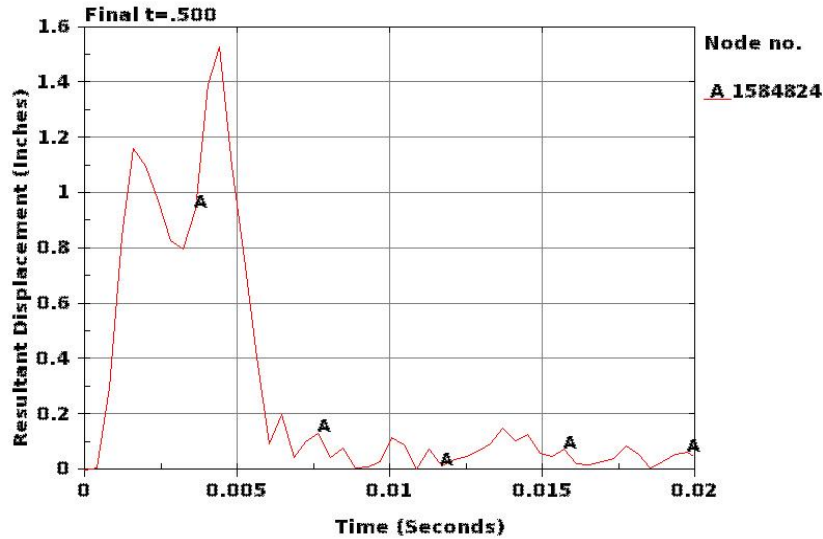


Figure 27.—Displacement time history at the location of maximum deflection.

For comparison, a shielding thickness required for containment was also calculated using the empirical UEDDAM equation (Ref. 1).

$$V = \sqrt{\frac{2LC_s t^2}{m \cos^2 \theta}} \quad (2)$$

The empirical material constant, C_s , for T700S/PR520 braided composite of 61,060 lb/in.² (421 MPa) was calculated based upon the impact test data shown in Figure 13. (V is the penetration velocity, t is the target thickness, m is the projectile mass, and θ is the obliquity angle.) Using the fragment presented perimeter, L , measured as shown in Figure 28, a required shielding thickness of 0.53 in. was calculated. The 0.53 in. UEDDAM thickness is in good agreement with the LS-Dyna required thickness of 0.500 in. Considering that both the UEDDAM and LS-DYNA required thicknesses are partially dependent upon the test data shown in Figure 13, this good agreement is not surprising.

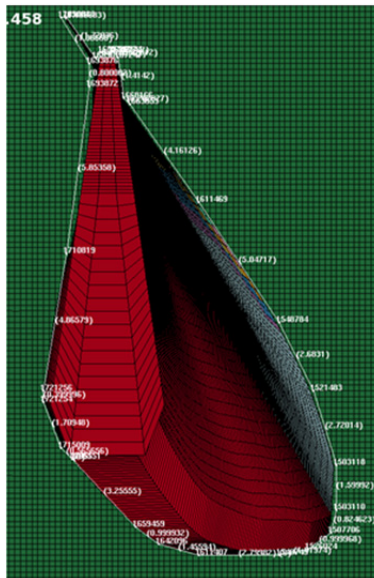


Figure 28.—Perimeter calculation for UEDDAM equation.

An estimate of the shielding requirements, for locations other than the worst-case location, was made using the UEDDAM equation. Using the UEDDAM significantly reduced analytical time compared to the more rigorous LS-DYNA impact analysis. It was acceptable to use the UEDDAM equation because of the reasonably good agreement with the LS-DYNA analysis presented above. The equation was used to evaluate the shielding requirement for several lower incident angle impacts. For each of the impact angles examined, the blade finite element model was positioned using the results of the trajectory analysis, and the blade fragment presented perimeter was calculated. The required shielding thickness for each of these impact conditions was then calculated using the UEDDAM procedure. Finally, the results were grouped into regions where shielding thicknesses between 0.35 and 0.5 in., and below 0.35 in. were required.

8.0 Weight Estimate

The width (longitudinal direction of aircraft) of the required fuselage shielding was calculated using the current FAA rule requiring a $\pm 3^\circ$ dispersion angle for disc burst evaluation since the results of the trajectory analysis showed that aerodynamic forces would not cause a blade dispersion greater this amount. Consideration of conditions not currently required under current FAA containment rules, such as multiple foreign object impacts and ricochets, were also not considered in this study. As a result, a clean blade release was assumed, along with no debris striking the blade which might cause the blade trajectory to be modified.

The $\pm 3^\circ$ dispersion from the release location for the worst-case impact leads to a ± 6.3 -in. displacement from the plane of rotation. The width of the blade perpendicular to the plane of rotation is ~ 10.2 in. Combining the dispersion distance with the blade width leads to a required shielding width of 22.8 in. For the weight evaluation in this study, the width of the shielding was rounded up to 24 in., as shown in Figure 29. No weight credit is taken for the potential overlap of forward and aft shielding areas.

The center of the shielding for the forward rotor should be placed ~ 2 in. forward of the blade plane of rotation. As discussed in Section 3.0, there are two effects causing a consistent forward travel of the blade. First, the blade travels forward due to the location of the blade mass center of gravity. Second, the aerodynamic forces also consistently cause the blade to move forward.

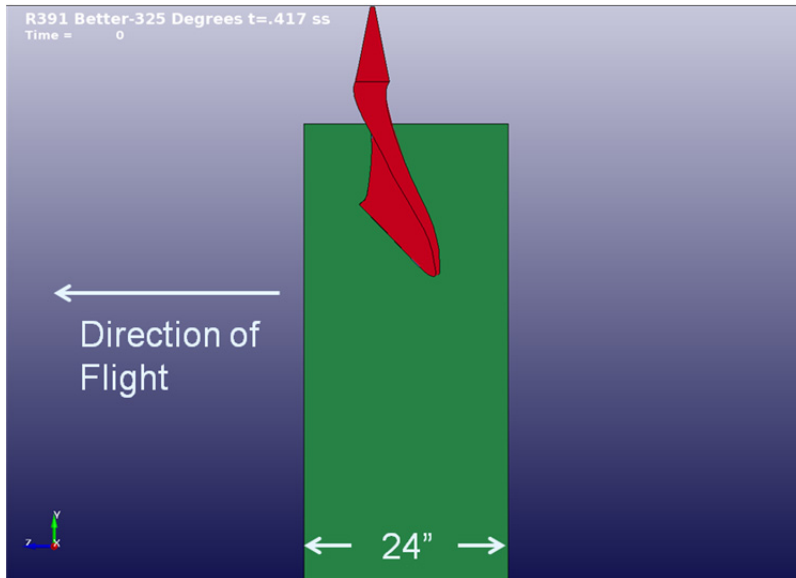


Figure 29.—Blade impact orientation with 24 in. shielding.

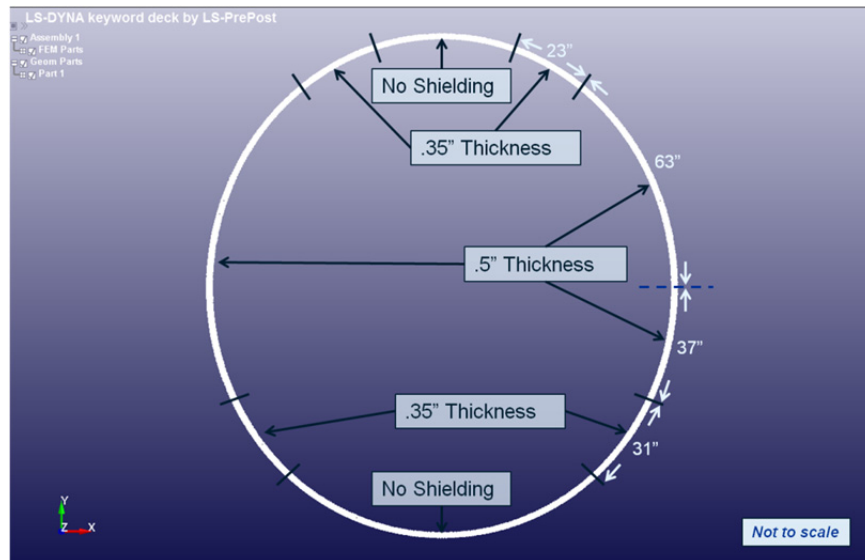


Figure 30.—Required shielding thickness regions.

Figure 30 shows the required shielding thickness to prevent blade penetration. Areas on the top and the bottom of the fuselage cannot be impacted, so no shielding is required in these regions. Additionally, areas adjacent to the top and bottom of the fuselage incur only lower angle blade impacts so less shielding is required than for areas that take more direct blade impacts. As discussed in the previous section, the UEDDAM equation was used to categorize areas, which require shielding thicknesses of less than 0.5 in. In areas where more than 0.35 in., but less than 0.5 in. shielding was required, the shielding thickness was rounded up to 0.5 in. In areas where more than 0.0 in., but less than 0.35 in. of shielding was required, the shielding thickness was rounded up to 0.35 in. In Figure 30, the required shielding is only shown on the right hand side of the image. Since this study assumed a counter-rotating configuration, blades would rotate both clockwise and counter-clockwise, and so identical shielding requirements on the left and right side of the fuselage were also assumed. In the study configuration, the engine is located vertically higher than the fuselage centerline, and so more shielding is required on the top half of the fuselage than the bottom half.

The circumferential length of the region requiring 0.50 in. of shielding was ~100 in. per side. With the required shielding width of 24 in., the total shielded surface area for either the forward or the aft rotor is 4,800 in.². Using a density of 0.0645 lb/in.³ for the T700S/PR520 composite, the required shielding weight is ~155 lb for each rotor. The circumferential length of the region requiring a thickness of 0.35 in. was ~54 in. per side. With the required width of 24 in., the area for either the forward or aft rotor is 2,592 in.². The resulting shielding weight is ~59 lb for each rotor. Adding the weights of 0.5 in. and 0.35 in. thick shielded regions gives a total shielding weight of ~214 lb for each rotor. Adding the forward and aft counter-rotating rotor shielding weights together yields a total weight of ~428 lb. As mentioned previously, because no specific distance between the forward and aft rotors was assumed, there was no assumed overlap between shielded areas.

If a portion of the composite shielding can serve both shielding and fuselage structural functions, then the weight specifically attributed to shielding may be reduced. Using a part of the composite structure for a dual purpose is a reasonable assumption considering the structural properties of the T700S/PR520 composite material. Assuming a fuselage thickness required to meet structural requirements of 0.2 in. (as was done in the FAA Open-rotor Analysis (Ref. 11)) over the total shielded area of 7,392 in.², leads to an estimated fuselage weight of ~95 lb for each rotor. Subtracting the 95 lb weight from the total shielding weight reduces the additional weight required for shielding each rotor to ~118 lb, or ~236 lb for the complete counter-rotating configuration. The fixtures that would be required to attach the shielding to the fuselage would be airframe specific. As a result, the potential additional weight required for these attachments has not been estimated. These attachment fixtures, and the shielding, would not need to be in the primary load path of the fuselage. Therefore, they should only be required to support the shielding, and should not add significant weight.

9.0 Summary

A detailed estimate for the fuselage shielding weight required to protect against an open-rotor blade loss has been made. This estimate was generated using a two-step procedure. First, a trajectory analysis was performed to determine the blade orientation and velocity at impact with the fuselage. Second, a finite element impact analysis was performed to determine the required fuselage thickness to prevent blade penetration. The impact analysis was conducted using an Federal Aviation Administration (FAA) provided composite blade geometry. The fuselage geometry was based on a medium-sized passenger airframe. Both the blade and fuselage utilized T700S/PR520 composite material. The estimated additional weight required for fuselage shielding for a counter-rotating open-rotor blade is ~236 lb per aircraft. This estimate is based on the shielding material serving the dual use of shielding and fuselage structure. If the shielding material is not used for dual purpose, and is only used for shielding, then the additional weight per aircraft is ~428 lb. A blade impact dispersion angle of $\pm 3^\circ$ was used for the weight estimate.

References

1. Lundin, Steven J., and Mueller, Richard B., *Advanced Aircraft Materials, Engine Debris Penetration Testing*, DOT/FAA/AR-03/37, December 2005.
2. Littell, Justin, *The Experimental and Analytical Characterization of the Macromechanical Response for Triaxial Braided Composite Materials*, PhD Dissertation, U of Akron, December 2008.
3. Littell, Justin D., Binienda, Wieslaw K., Goldberg, Robert K., and Roberts, Gary D., *Characterization of Damage in Triaxial Braid Composites Under Tensile Loading*, NASA/TM—2009-215645.
4. Kohlman, Lee W., *Evaluation of test methods for triaxial braid composites and the development of a large multiaxial test frame for validation using braided tube specimens*. Ph.D. Dissertation, The University of Akron, Akron, Ohio, 2012.

5. Pereira, J. Michael, Roberts, Gary D., Ruggeri, Charles, R., Gilat, Amos, and Matrka, Thomas, *Experimental Techniques for Evaluating the Effects of Aging on Impact and High Strain Rate Properties of Triaxial Braided Composite Materials*, NASA/TM—2010-216763.
6. Littell, J.D.; Binienda, W.K.; Arnold, W.A.; Roberts, G.D.; and Goldberg, R.K.: *Effect of Microscopic Damage Events on Static and Ballistic Impact Strength of Triaxial Braid Composites*. Composites Part A: Applied Science and Manufacturing, Vol. 40, pp. 1846-1862, 2009.
7. Goldberg, R.K.; Blinzler, B.J.; and Binienda, W.K.: *Modification of a Macromechanical Finite-Element Based Model for Impact Analysis of Triaxially Braided Composites*, Journal of Aerospace Engineering, Vol. 25, pp. 383-394, 2012.
8. Blinzler, B.J.; Goldberg, R.K.; and Binienda, W.K.: *Macro Scale Independently Homogenized Subcells for Modeling Braided Composites*, AIAA Journal, Vol. 50, pp. 1873-1884, 2012.
9. Envia, Edmane, *Open Rotor Aeroacoustic Modelling*, NASA/TM—2012-217740.
10. Hallquist, John O., editor, *LS-DYNA 971 R6.1.0 Keyword Manual*, August 2012.
11. Fankenberger, Chuck, and Phillips, Raena, *Open Rotor Analysis*, Naval Air Warfare Center Weapons Division Presentation, September 2012.
12. Schweizerhof, K., K. Weimar, Th. Munz, and Th. Rottner. *Crashworthiness Analysis with Enhanced Composite Material Models in LS-DYNA – Merits and Limits*. LS-DYNA World Conference. 1998, Detroit, MI, USA.
13. Matzenmiller, J. Lubliner, and R.L. Taylor. *A constitutive model for anisotropic damage in fiber-composites*. Mechanics of Materials 20, 1995, p. 125-152.
14. Modeling Guidelines Document Version 12-1 Dated June 1, 2012, <http://awg.lstc.com/>
15. Carney, K., Melis, M., Fasanella, E., Lyle, K., Gabrys, J., *Material Modeling of Space Shuttle Leading Edge and External Tank Materials for Use in the Columbia Accident Investigation*, 8th International LS-DYNA User's Conference, 2004.
16. Carney, K., Pereira, M., Revilock D., and Matheny P., *Jet Engine Fan Blade Containment Using an Alternate Geometry and the Effect of Very High Strain Rate Material Behavior*, International Journal of Impact Engineering, Vol. 36, pp. 720-728, 2009.

Appendix—Propeller Blade to Fuselage Impact History

In conjunction with the analysis presented in Section 4.0 of this report, an investigation to locate trajectory information from historical aircraft accidents and incidents was made. This study was conducted with the National Transportation Safety Board (NTSB) and the Federal Aviation Administration (FAA) reviewing available information and compiling it to determine the history of released blade trajectories and likely impact points on the aircraft. A review was performed by the NTSB which included 12 incidents between 1990 and 2008. In this query of the data base, many of the events did not include information about fuselage impact, and some that did mention damage did not clearly identify the location of the damage. In the review, “plane of rotation” is often the location given when fuselage impact location is mentioned.

Events of note are:

- On March 5, 1967, a Convair 340 accident occurred in Marseilles, Ohio. Accident report NTSB 1967-03-05-US.pdf report states—“Investigation revealed that all four blades of the right propeller separated in flight and the No. 2 blade penetrated the aircraft fuselage in line with the propeller plane. The penetrations destroyed the structural integrity of the fuselage to an extent that, together with the loads caused by a right yaw which accompanied the propeller separation, the fuselage failed along the line of penetrations and the aircraft crashed.”
- On February 8, 1976 a DC6 incident is reported in NTSB-AAR-76-17, which states—“The failed blade penetrated the fuselage near station 261 and traversed the width of the aircraft’s fuselage”. AC20-52 indicates that the ice shield on a DC-6 runs from fuselage station 240 to station 280. Therefore the blade impacted one inch aft of the center of the ice shield.
- On July 14, 1990, a Lockheed Electra L-188A accident occurred in Aruba and is reported in MIA90-LA-153 which states—“a portion of a propeller camber sheet which had cut thru the airplane and was lodged in the fuselage in the plane of rotation of the No. 3 propeller”.

The database is limited in specific measurements; angles and precise measurements are not available. The limited data in the reports indicate that the released blade or blade fragment travels “in the plane of rotation”. The lack of containment structure allows the blade to travel tangent to the rotation with small deviations for aerodynamic loading. There does not appear to be a need for protection over a large fore and aft dispersion angle from this limited information, supporting the conclusions of Section 4.0. All of the events provided by the NTSB are contained in Table 5.

TABLE 5.—HISTORICAL PROPELLER RELEASE EVENTS PROVIDED BY NTSB

Date	NTSB Incident No.	Damage noted in record
7/14/1990	MIA90LA153	Damage to fuselage in the plane of rotation of the No3 Propeller
7/25/2000	MIA00LA225	Propeller separation, not blade failure, improper assembly
5/19/2000	DEN00FA092	Damage to fuselage, Right Wing and Ring wing flap Lox unknown
8/15/1999	NYC99LA202	No damage to fuselage
9/19/1998	FTW98FA392	No mention of damage from released blade
12/9/1990	SEA91LA031	Propeller separation, angle of impact to nose not defined
6/1/1991	NYC91LA153	Propeller separation no fuselage impact
11/22/1991	CHI92LA031	Two Propeller blades separated and damaged nose, angle not defined
8/18/1992	NYC92LA166	Propeller blade separated and penetrated the fuselage, angle not defined
4/24/2001	CHI01FA128	Crankshaft failed and the complete propeller separated and struck empennage
3/21/1997	ANC97LA046	Blade tip separated, penetrated nose and impacted other engine nacelle. Angle not defined
6/8/2008	CHI08LA160	Blade tip separated and impacted nose, angle not defined